Thermal behavior study of pristine and modified halloysite nanotubes: a modern kinetic study

Celia Duce[a], Stefano Vecchio Cipriotti[b,*], Lisa Ghezzi[a], Vincenzo Ierardi[c], Maria Rosaria Tinè[a]

[a]Dipartimento di Chimica e Chimica Industriale, Università di Pisa, Via Moruzzi, 56124 Pisa, Italy
[b]Dipartimento S.B.A.I., Sapienza University of Rome, Via del Castro Laurenziano 7, 00161 Roma, Italy
c aggiungere

Abstract

Pristine halloysite nanotubes (HNTs) were studied by thermogravimetry (TG) up to 800°C. Etching of alumina from inside the tube (causing a significant increase of tube lumen) was realized by treating the material with an acidic H_2SO_4 solution at 50°C. Both materials were characterized by TG-FTIR techniques and their thermal behaviors were compared with that of kaolinite (KAO). The coupling of TG with FTIR enables to detect the gases evolved during the TG experiments, thus confirming that only pristine HNTs undergo dehydration with the loss of interlayer water molecules at around 245°C, while dehydroxylation occurs in all these materials in close temperature ranges around 500°C. TG runs at five different heating rates (2, 5, 10, 15 and 20 °C min^{-1}) were carried out in the same experimental conditions used for the thermal analysis study with the aim to investigate dehydration and dehydroxylation kinetics using some isoconversional methods, recommended by the ICTAC kinetic committee, and a modulated thermogravimetry heating rate method. Finally, the results of the kinetic analysis were discussed and explained in terms of the strengths of the hydrogen bonds broken during these processes.

*Corresponding Author (S. Vecchio Cipriotti)
E-mail Address: stefano.vecchio@uniroma1.it

Introduction

Halloysite is a two-layered alumosilicate clay with chemical formula $Al_2Si_2O_5(OH)_4 \times nH_2O$, consisting of Si-tetrahedral outer sheets joined to Al-octahedral inner sheets by planes of oxygen atoms of tubular shape. Its structure is made up of nano-size tubes having external diameter of 50-80 nm, cylindrical pore (lumen) of 10-15 nm and length of about 1000 nm [1]. Due to this characteristic shape and the presence of less abundant surface hydroxyl groups (with respect to kaolin and montmorillonite) halloysite nanotubes (HNTs) can be dispersed in polymers without the need of exfoliation to form halloysite-polymer composites that are transparent in wide ranges of wavelengths, including near-UV [1-4]. In addition, HNTs is not hazardous for the environment and is available in large amount (thousand of tons) at a very low cost. The outer and inner structure is made up of polar compounds (sheets of $[SiO_4]$ tetrahedra and sheets of edge-sharing $[AlO_6]$ octahedra), thus providing a good hydrophilicity and therefore a good dispersion in polar polymers, like epoxy, polyethyleneimine, polyamides, polyacrylates, polyvinyl alcohol and biopolymers, like starch, pectin, chitosan, and humic acid [5-10]. Due to their elongated shape and cylindrical lumen, natural HNTs can be loaded with several chemically and biologically active substances [4], like drugs [3,11], proteins [3,12], DNA [13], antibacterials [14], cosmetics [15], thus providing useful bionanocomposite materials for their controlled release for pharmaceutical applications. Sulfuric acid treatments have been provided as an efficient method for enlargement of HNTs lumen diameter with the aim to increase the tube loading capacity. The selective etching of alumina sheets was optimized by tuning time, temperature, and acid concentration; in particular at high level of etching (above 30-40% of dealumination) halloysite gradually loses its tubular morphology [16].

Nowadays it is not clear how HNTs are formed in nature. According to some authors, kaolinite (KAO), with a layer structure consisting of superimposed silicon tetrahedral sheets and aluminum octahedral sheets, is the main mineral phase of kaolin having the same chemical formula of halloysite. It is demonstrated that KAO may roll leading to the formation of HNTs [17]. KAO is an important material used in several industrial processes like food-processing industry, oil shale processing,

ceramic industry, as a pozzolanic material or as a filling agent, and for its use it is pre-heated at high temperature (from 450 to 700°C) until it is transformed to metakaolin via dehydroxylation [18]. Dehydroxylation, elimination of water from hydroxyl groups, is an important thermal dissociation reaction among those occurring in the kaolinite group minerals and in natural or synthesized silicate materials [19]. Non-isothermal kinetics of this process, which occurs at temperature quite higher than dehydration due to the presence of stronger hydrogen bonds between the OH groups, was extensively studied for different type of KAOs [18,20-24], but little is known about the same process occurring in HNTs where early papers used questionable methods under isothermal conditions [25,26].

Some authors adopted in their studies [21b-c,24] kinetic approaches (in particular, model-fitting methods) that the ICTAC kinetics committee demonstrated to provide unreliable results [27]. Furthermore, Liu and co-worked recently applied an early method to study dehydroxylation of synthetic Al-goethite, providing unreasonable low activation energies between 3 and 7 kJ mol^{-1} [28]. Therefore, a first aim of this study is to investigate the thermal behavior of pristine and modified via lumen enlargement HNTs and to compare it with that of KAO. A second aim is to provide an exhaustive description of kinetic analysis of both dehydration (for HNTs only) and dehydroxylation processes occurring in pristine and modified HNTs (treated at 50°C with sulfuric acid), with a view to correlate the results obtained with the different structures of these materials. In particular the coupling of thermogravimetry (TG) with FTIR enabled to completely characterize the thermal degradation of HNTs (both pristine and etched) whereas TG experiments performed at different heating rates were used for the kinetic study. The data so obtained were analysed by several isoconversional methods and compared with those obtained by modulated thermogravimetry.

Theoretical background

The kinetic description of thermally stimulated processes occurring in materials in the condensed phase is rather more complex than that for homogeneous reactions. The first difficulty arises from the

definition of the function describing the progress of the reaction against time (under isothermal condition) or temperature (under the most commonly used non-isothermal condition with constant heating rate β=dT/dt). The so-called degree of conversion α, which is 0 at the initial temperature T_i and 1 at the final temperature T_f of each step, is defined as $\alpha=(m_i-m_T)/(m_i-m_f)$, where m_i, m_f and m_T are the sample masses at the corresponding T_i, T_f and T according to thermogravimetric (TG) data.

The explicit dependence of the reaction rate by both the absolute temperature and the extent of conversion α, strictly valid under the assumption of a of a single-step process, is expressed by the following equation

$$\frac{d\alpha}{dt} = k(T)f(\alpha) \quad (1)$$

where $k(T)$ usually represents the rate constant, commonly used in the form of the Arrhenius equation that enable to re-write Eq. (1) in the following form

$$\frac{d\alpha}{dt} = Ae^{-E/RT}f(\alpha) \quad (2)$$

where A is the pre-exponential factor, E is the activation energy and $f(\alpha)$ is a function called reaction model [29,30].

For experiments carried out under modulated heating rate conditions using an oscillatory temperature program (temperature increases “smoothly varying temperature sine wave” [31]), the ratio between the reaction rates expressed in Eq. (2) and calculated at the peak and valley of the sinusoidal wave form (α_p and α_v), can be derived as follows:

$$\frac{d\alpha_p/dt}{d\alpha_v/dt} = \frac{e^{-E/RT_p}f(\alpha_p)}{e^{-E/RT_v}f(\alpha_v)} \quad (3)$$

where the $\ln((\alpha_p/\alpha_v)$ signal is obtained using a Fourier transformation. Under constant conversion condition (or at least for small variation between adjacent peaks and valley) the ratio $f(\alpha_p)/f(\alpha_v)$ approaches unity, being $f(\alpha_p)\approx f(\alpha_v)$. Taking the logarithm of both sides of Eq. (3) and solving for E yields:

$$E = \frac{RT_pT_v ln(d\alpha_p/d\alpha_v)}{T_p - T_v} \quad (4)$$

In any oscillatory temperature program, T_p and T_v are defined as $T_p = \langle T \rangle + A$ and $T_v = \langle T \rangle - A$, where $\langle T \rangle$ is the average temperature, A is the temperature amplitude, while $T_p - T_v = 2A$. Eq. (4) can be further simplified by introducing a new parameter L, which is set equal to the peak-to-peak amplitude of the ln(dα) signal (L = ln dα_p – ln dα_v). Once the values have been replaced in Eq. (4), it assumes the following more simple form:

$$E = \frac{R(T^2 - A^2)L}{2A} \quad (5)$$

It is worth noting that a kinetic method based on Eq. (5) is among those called "model-free", as its computations do not depend on the knowledge of the choice of a proper model function $f(\alpha)$.

On the other hand, approaches based on multiple heating rate (or temperature) programs are highly recommended by the ICTAC Kinetic Committee [32]. The time dependency of reaction rate dα/dt is then replaced by its corresponding temperature dependency dα/dT = β^{-1} dα/dt reaction rate, giving Eq. (6):

$$\frac{d\alpha}{dT} = \left(\frac{A}{\beta}\right) e^{-E/RT} f(\alpha) \quad (6)$$

Separation of variables in Eq. (6) yields:

$$\frac{d\alpha}{f(\alpha)} = \left(\frac{A}{\beta}\right) e^{-E/RT} dT \quad (7)$$

The integrals of both the left- and right-hand side of Eq. (7) gives:

$$\int_0^\alpha \frac{d\alpha}{f(\alpha)} = g(\alpha) = \left(\frac{A}{\beta}\right) \int_0^T e^{-E/RT} dT \quad (8).$$

The temperature integral in Eq. (8) has no exact analytical but approximate solutions that give rise to some of the most commonly isoconversional methods, whose equations for each fixed extent of conversion α have the following general form:

$$ln\left(\frac{\beta}{T^B}\right)_\alpha = Const - C\left(\frac{E}{R}\right)\left(\frac{1}{T_\beta}\right)_\alpha \quad (9)$$

where B and C are adjustable parameters, whose values depend on the approximation made. In particular, for the Ozawa-Flynn-Wall (OFW) method [33,34], based on the Doyle's approximation [35], B=0 and C=1.052. More accurate results can be obtained using the Kissinger-Akahira-Sunose (KAS) method [36], where B=2 and C=1 or the Starink (STA) method [37] (B=1.92 and C=1.008). Each value of activation energy at each given extent of conversion is calculated from the slope of the regression line obtained by plotting the left-hand side of Eq. (9) against the reciprocal temperature $(T_\beta^{-1})_\alpha$. Isoconversional methods, along with the invariant kinetic parameters [38,39] and the constant rate thermal analysis (CRTA) [40,41], are recognized to be among those who usually give reliable results and relevant books, review and papers [27,29,42,43] deal with the advantage of their use. These methods are based on the assumption that the reaction rate at constant degree of conversion is only a function of temperature. Vyazovkin developed a method (VYA) that gives results with a better accuracy by numerical integration of the right-hand side of Eq. (5) [44-46] by minimizing the following function:

$$\phi(E_\alpha) = \sum_{i=1}^{n}\sum_{j\neq i}^{n}\frac{J[E_\alpha, T_i(t_\alpha)]}{J[E_\alpha, T_j(t_\alpha)]} \quad (10)$$

where $J[E_\alpha, T(t_\alpha)] = \int_0^{T_\alpha}\exp[-E_\alpha/RT(t)]\mathrm{d}T$ is solved numerically and minimization is made for each value of α with the aim to obtain a conversion dependency of activation energy. The reaction model and the α-dependence of pre-exponential factor ($\ln A_\alpha$) can be accurately determined only in the case of processes that follow approximately a single-step kinetics, for which it can be expected that activation energy does not varies appreciably over the entire range of the extent of conversion α by combining the results of isoconversional (model-free) and model-fitting methods [47]. By applying a model-fitting method (Coats-Redfern [48] in this study) a pair of Arrhenius parameters can be obtained for each reaction model using a single-heating rate experiment. Wide ranges of values are found for both parameters when all the reaction models are considered, but a strong linear correlation

denoted as compensation effect is found between them in the following form:

$$lnA_i = aE_i + b \quad (11)$$

where the subscript i refers to each of all the reaction model. Once a and b parameters have been determined at each heating rate using a linear regression procedure, these values were replaced in Eq. (11) by their mean values <a> and <b> while the E_i values were replaced by the isoconversional values of E_α to determine the corresponding values of $\ln A_\alpha$ for each given value of α [47].

Experimental

Materials

Kaolinite and pristine halloysite nanotubes were purchased from Sigma Aldrich and used without further purification. The procedure followed for the HNT lumen etching was similar to that reported in literature [16]. A suspension of halloysite was obtained by dispersing 5 g of Halloysite in 300 ml of a 2 mol l^{-1} H_2SO_4 solution. The suspension was magnetically stirred for 48 hours on a hot plate at the controlled temperature of 50 °C. The processed halloysite was then washed with distilled water until the pH of the supernatant from the washing stage was in the range 6-7, similar to that of pure halloysite suspension. The sample was dried in an oven at 50°C and then characterized by TG.

Instruments

Samples were analyzed through scanning electron microscopy (SEM) and scanning transmission electron microscopy (STEM). Images were collected using an Ultra High Resolution Field Emission Scanning Electron Microscopy (UHR-FE-SEM) by Zeiss equipped with a STEM. In order to collect SEM images, powder of pristine and etched HNTs have been deposited onto a substrate of copper. Instead the STEM samples were prepared using as substrate a TEM grid.

All the TG experiments were performed using a TA Instruments Q5000IR thermogravimetric instrument equipped with an FTIR (Agilent Technologies) Cary 640 spectrophotometer for Evolved

Gas Analysis (EGA). The Q5000IR thermogravimetric analyzer has the optional capability to work in modulated mode (modulated thermogravimetry, MTG). TG measurements were performed in this study with both dynamic conventional (constant heating rate) and modulated temperature programs. Both types of experiments were carried out from 40 to 800 °C using Pt crucibles under a stream of air of 25 ml min^{-1}. In conventional TG, samples were heated at five different heating rates (2, 5, 10, 15, 20 °C min^{-1}) to process TG data for kinetic computations. In MTGA experiments samples were heated at a heating rate of 2° C min^{-1} with a temperature modulation amplitude of ± 5°C and a period of 200 s. The MTG curves were analyzed using the TA Universal Analysis 2000 software. TG-FTIR measurements were performed at a rate of 20 °C min^{-1}, from 40 °C to 800 °C under air flow (70 ml min^{-1}), from 600 to 3000 cm^{-1} with a 4 cm^{-1} width slit. To reduce the background absorption from water and carbon dioxide in the atmosphere, the optical bench was purged with nitrogen. In addition, a background spectrum was taken before each analysis in order to zero the signal in the gas cell and to eliminate the contribution due to the amount of ambient water and carbon dioxide. The amount of sample in each TG and TG-FTIR measurement varied between 4 and 8 mg.

Results and discussion

Treatments with sulfuric acid have been provided as an efficient method for enlargement of HNTs lumen diameter with the aim to increase the tube loading capacity [16]. The increase of the HNTs lumen, after acidic treatment, is clearly evident in Fig. 1, where it is possible to see some examples of SEM and STEM images of pristine and etched HNTs. STEM combines the principles of transmission electron microscopy and scanning electron microscopy. Its primary advantage over conventional SEM imaging is the improvement in spatial resolution with consequently better imaging resolution.

Fig. 1a-b shows the STEM images of pristine and etched HNTs, respectively. The arrows and the dashed lines highlight the size of the HNT lumen, which, in the case of pristine HNTs, is 15-20 nm; while in etched HNTs, because of the etching process, increases up to 30-40 nm. The enlargement of

lumen size is further supported by SEM images (Fig. 1c-d). As could be expected the images of etched HNTs (Fig. 1b,d) show changes in halloysite morphology. Indeed, although the rodlike structure was preserved, the etched tubes present broken points and the halloysite walls appear more friable and porous.

The TG/DTG curves of pristine HNTs, etched HNTs and KAO are given in Fig. 2. Relevant data taken from these measurements (peak DTG temperatures and mass loss percentages) of each step are shown in Table 1. The thermal behavior of HNTs and etched HNTs showed remarkable differences. In particular, pristine HNTs undergo four steps of mass loss, the first of which at T_p=37.5 °C (mass loss 2.3%) is due to water physically adsorbed to the surface, while the second, in the range 200-285 °C (mass loss 3.3%), is ascribed to the release of interlayer water molecules bound by hydrogen bonds. The third step is due to dehydroxylation (condensation of hydroxyl groups of aluminum inner sheets) around 470°C (mass loss 11.4%), while at 744°C the mass loss of 1.7% is ascribed to the release of SO_2 due to the thermal decomposition of sulfides (as impurity) or alunite, according to what it was recently reported in literature [20,49], even for kaolin [50]. The hypothesis that the mass losses below 500°C could be exclusively due to water release, is confirmed by FTIR analysis. The gas evolved at the fixed temperatures of 37.5, 245 and 468 °C present the same spectrum (see Fig. 3a) showing the narrow bands at 4000-3500 and 2000-1300 cm^{-1} typical of the spectrum of water [51]. On subsequent heating, the spectrum recorded at 750°C (Fig. 3b) shows the characteristic bands of SO_2 impurities (1390, 1338 and 1180 cm^{-1}) [51, 52].

By contrast, etched HNTs did not show the loss of interlayer water around 245°C, thus demonstrating that the acidic etching at 50°C, responsible for the enlargement of HNTs lumen [16], caused the elimination of the interlayer water. The water loss attributed to dehydroxylation takes place at temperature slightly higher (T_p at 479°C instead of 468 °C), and with a lower mass loss (6.0% instead of 11.4%) than in pristine HNTs. As expected, around 730°C the loss of SO_2 is confirmed also in etched HNTs. No dehydration is shown for KAO that is stable up to 330 °C in agreement with the results reported in [53], while other authors found in the temperature range up to 150°C a slight mass

loss due to dehydration [20,21c]. Dehydroxylation occurs in a single step in the wide temperature range between 400 and 700°C in agreement with literature findings [18,20,21c,22,50].

Eqs. 10 and 11 were considered to apply the four isoconversional methods denoted as OFW, KAS, STA and VYA to analyze the kinetics of dehydration in HNTs by processing TG data between 200 and 280°C (Fig. 2), and dehydroxylation in HNTs, etched HNTs and KAO in the temperature range close to 470-500°C. The results of kinetic analysis regarding dehydration and dehydroxylation, reported as the usual conversion dependency of activation energy, are summarized in Figs. 4 and 5, respectively. Interpretation of these results should be made in terms of the energy barrier to be overcome by water molecules to proceed with dehydration or dehydroxylation. Application of OFW, KAS and STA methods to dehydration of HNTs seems to fail due to the significant change in E_α values preventing the use of Eq. (7) that implies separation of variables, and is rigorously valid only if neither the model function $f(\alpha)$ depends on temperature nor activation energy E_α on the degree of conversion. Furthermore, these results indicate a multi-step nature of the process investigated. However, the results of the VYA method, which can be applied even in the case of remarkable variation of E_α values, are in close agreement with those determined with the previous cited methods (in particular in the range $0.55<\alpha<0.95$, where E_α drops from 170 to 38 kJ mol^{-1}). It is worth noting that these values are markedly higher than the molar vaporization enthalpy of water (≈44 kJ mol^{-1}). On the other hand, the temperature range for the occurrence of this process (200-280°C) is remarkably higher than that of pure water. At this regard, water vaporization kinetics from bulk and from clays was recently investigated [54] and average values ranging from 43.8 to 56.2 kJ mol^{-1} were obtained for the former and the latter materials, respectively, because of the low temperature range of the occurrence of this process (from –20 to 90°C).

However, at the beginning of dehydration process of HNTs ($\alpha<0.30$) the E_α values obtained by the VYA method increase from 180 to 200 kJ mol^{-1} and then decreases to about 175 kJ mol^{-1}. Actually, these change of E_α values are not so high (slightly higher than the associated uncertainties) even if

they cannot be neglected. In general, increasing and decreasing trends of E_α values should be interpreted in terms of the increase of decrease of the energy barrier for the occurrence of the process examined. A decrease followed by an increase of water molecular mobility occurring during heating can be probably the main factor that generated those variation of E_α values. On the other hand, water molecular mobility is particularly affected by the rupture of weaker hydrogen bonds within the [AlO_6] octahedra inner sheets. Constant E_α values (≈171 kJ mol^{-1}) were found in the range $0.30 \leq \alpha < 0.60$, followed by a significant decrease to the values usually considered for free vaporization of pure water (40-45 kJ mol^{-1}). The decreasing trend of E_α values at the end of the process can be explained by the fact that the water molecular mobility increases up to values comparable to those found in bulk pure water. The results obtained with MTG, which adopted a differential isoconversional approach with respect to the integral one offered by OFW, KAS and STA, is completely in disagreement with those of all other methods considered at the beginning ($\alpha < 0.30$) and at the completion ($\alpha > 0.80$) of the process. A reasonable explanation of these large deviations can be ascribed to the approximation made in Eqs. (3-4) to consider $f(\alpha_p) \approx f(\alpha_v)$, which is reasonably valid in most of the conversion ranges. However, this approximation is inapplicable for n-th order models when the values of α approach unity and for the autocatalytic model function when α approaches either zero or unity (as in the case of dehydration of HNTs examined in this study) [31]. Slight higher values of E (of about 40 kJ mol^{-1}) are also found in the range $0.30 \leq \alpha < 0.80$, which are practically constant, similarly to what it is observed using all the other methods.

In Fig. 5a substantial agreement is found among the isoconversional dependencies of E_α values related to dehydroxylation determined using the five methods and the slight differences between the results of the first three integral approaches (OFW, KAS and STA) and those of VYA and MTG are limited to small ranges of α values. Large deviations of E values calculated using the MTG method when α approaches zero and unity is attributed (as in the case of dehydration of HNTs) to the failure of the approximation $f(\alpha_p) \approx f(\alpha_v)$ when a process (as probably in this case) can be described by a

autocatalytic model function [31]. Dehydroxylation in HNTs showed a trend similar to that of dehydration in the range up to α=0.40, followed by practical constant E_α values (around 190-200 kJ mol^{-1}), in close agreement (within a usual estimated uncertainty around 5-7%) with the single value found in literature (≈185 kJ mol^{-1}) [26]. As expected, quite higher E_α values are shown in the case of etched HNTs (Fig. 5b) and good agreements are found among the E_α values determined with the five methods applied (except in the case of the MTG method for α≈0 and α≈1). An increasing trend of E_α values can be attributed to a decreasing trend in molecular mobility of water (obtained by condensation of hydroxyl groups) during the course of the process, probably caused by the etching of [AlO_6] inner sheets. At a first sight, dehydroxylation of KAO (Fig. 5c) seems to be described in a more simple way, with superimposable and practically constant values of E_α determined by the five methods (around 220 kJ mol^{-1}) for α<0.6. A good agreement (at least in the range α<0,70) is found also with literature data on KAO [21c] and with the values determined for etched HNTs. Remarkable deviation of the E_α values determined with the MTG method is shown in the range α>0.8, ascribed to the above-cited failure of the approximation $f(\alpha_p)\approx f(\alpha_v)$, thus suggesting in this case that the mechanism of dehydroxylation of KAO can be reasonably described using n-th order models [31].

These findings, along with the comparison of their thermal behavior, suggest that the lumen enlargement caused by the acidic etching of the inner sheets of aluminum oxide provides a material even more similar to KAO than pristine HNTs.

Conclusions

Coupling of TG and FTIR techniques demonstrated in this study to be a useful tool to investigate the thermal behavior of both pristine and etched HNTs. The acidic etching of the [AlO_6] octahedra inner sheets of pristine HNTs is a common procedure used to enlarge the cylindrical lumens in order to load HNTs with suitable amounts of chemically and biologically active substances. SEM and STEM

techniques used in this study confirmed to be able in providing images proving indubitably that the etching of HNTs produced changes in halloysite morphology. Although the rodlike structure was preserved, the etched tubes presented broken points and the halloysite walls appeared more friable and porous. These structural changes are responsible of relevant changes in the thermal behavior of HNTs (*i.e.*, lost of layered water molecules) that appears more similar to kaolinite (tested only for comparison purpose) than to precursor. A modern kinetic analysis of both dehydration and dehydroxylation processes was performed in accordance with recent ICTAC recommendations. Different differential (MTG) and integral (OFW, KAS, STA and VYA) isoconversional methods confirmed the complex multi-step nature of both processes, evidenced by the non-negligible variation of E_α with increasing the degree of conversion. Increasing and decreasing trends of E_α values were interpreted in terms of increase and decrease of the molecular mobility of water hypothesized during the occurrence of these processes.

Acknowledgements

The authors acknowledge the financial support from FIRB 2012, *Clay nanotubes for designing eco-compatible smart materials*, funded by the Italian Ministry of University and Research (Project No.RBFR12ETL5) and Dr. Giuseppe Lazzara and Prof. Peter Simon for helpful discussions.

References

1. Du M, Guo B, Jia D. Newly emerging applications of halloysite nanotubes: a review. Polym. Int. 2010;59:574-95.
2. Price R, Gaber B, Lvov Y. In vitro release characteristics of tetracycline, khellin and nicotinamide adenine dinucleotide from halloysite; a cylindrical mineral for delivery of biologically active agents. J. Microencapsul. 2001;18:713-23.
3. Abdullayev E, Lvov Y. Clay nanotubes for corrosion inhibitor encapsulation: release control with end stoppers. J. Mater. Chem. 2010;20:6681-7.
4. Abdullayev E, Lvov Y. Clay nanotubes for controlled release of protective agents – a review. J. Nanosci. Nanotechnol. 2011;11:10007-26.
5. Liu M, Guo B, Du M, Cai X, Jia D. Properties of halloysite nanotube-epoxy resin hybrids and the interfacial reactions in the systems. Nanotech. 2007;18: 455703/1-9.
6. Abdullayev E, Lvov Y. Halloysite clay nanotubes as a ceramic “skeleton” for functional biopolymer composites with sustained drug release. J. Mater. Chem. B 2013;1:2894-903.
7. Lvov Y. Price R, Gaber B. Thin film nanofabrication via layer-by-layer adsorption of tubule halloysite, spherical silica, proteins and polycations. Coll. Surf. A 2002;198-200:375-82.
8. Liu M, Guo B, Du M, Jia D. Drying induced aggregation of halloysite nanotubes in polyvinyl alcohol/halloysite nanotubes solution and its effects on propertiesof composite films. Appl. Phys. A 2007;88:391-5.
9. Wei W, Abdullayev E, Hollister A, Mills D, Lvov Y. Clay nanotube/poly(methyl methacrylate) bone cement composite with sustained antibiotic release. Macromol. Mater. Eng. 2012;297:645–53.
10. Cavallaro G, Lazzara G, Milioto S. Dispersions of nanoclays of different shapes into aqueous and solid biopolymeric matrices. Extended physico-chemical study. Langmuir 2011;27:1158–63.
11. Veerabadran N, Price R, Lvov Y. Clay nanotubes for encapsulation and sustained release of drugs. NANO 2007;2:215–22.
12. Shchukin D, Price R, Lvov Y. Biomimetic synthesis of vaterite in the interior of clay nanotubules. Small 2005;1:510–3.
13. Shamsi MH, Geckeler KE. The first biopolymer-wrapped non carbon nanotubes. e-Nanotech 2008;19:1–5.
14. Joshi A, Abdullayev E, Vasiliev A, Volkova O, Lvov Y. Interfacial modification of clay nanotubes for the sustained release of corrosion inhibitors. Langmuir 2013;29:7439–48.

15. Suh Y, Kil D, Chung K, Abdullayev E, Lvov Y, Mongayt D. Natural nanocontainer for the controlled delivery of glycerol as a moisturizing agent. Journal of Nanoscience and Nanotechnology 2011;11:661–5.
16. Abdullayev E, Joshi A, Wei W, Zhao Y, Lvov Y. Enlargement of Halloysite Clay Nanotube Lumen by Selective Etching of Aluminium Oxide. ACSNANO 2012;6(8):72167226.
17. Singh B. Why does halloysite roll? – a new model. Clays and Clay Minerals 1996;44:191–6.
18. Gasparini E, Tarantino S.C., Ghigna P, Riccardi MP, Cedillo-González EI, Siligardi C, Zema M. Thermal dehydroxylation of kaolinite under isothermal conditions. Appl Clay Sci. 2013;80-81:417–25.
19. Vecchio Ciprioti S, Catauro M. Synthesis, thermal behavior and FTIR study of some calcium silicate gel-glasses of general formula $xCaO\cdot(1–x)SiO_2$. Kinetic analysis of their dehydration and dehydroxylation processes. Submitted to Thermochimica Acta, 2014.
20. Cheng H, Yang J, Liu Q, Frost RL. Thermogravimetric analysis–mass spectrometry (TG–MS) of selected Chinese kaolinites. Thermochim. Acta 2010;507-508:106–14.
21. Ptácek P, Soukal F, Opravil T, Havlica J, Brandstetr J. The kinetic analysis of the thermal decomposition of kaolinite by DTG technique. Powder Technol. 2011;208:20-5; Ptácek P, Soukal F, Opravil T, Nosková M, Havlica J. The non-isothermal kinetics analysis of the thermal decomposition of kaolinite by effluent gas analysis technique, Powder Technol. 2010;203:272–6; Ptácek P, Kubatova D, Havlica J, Brandstetr J, Soukal F. Isothermal kinetic analysis of the thermal decomposition of kaolinite: the thermogravimetric study. Thermochim Acta 2010;501:24–9.
22. L'vov BV, Ugolkov VL. Kinetics and mechanism of dehydration of kaolinite, muscovite and talc analyzed thermogravimetrically by the third-law method. J Therm Anal Calorim. 2005;82:15–22.
23. González Sánchez F, Van Loon LR, Ginni T, Jakob A, Glaus MA, Diamond LW. Self-diffusion of water and its dependence on temperature and ionic strength in highly compacted montmorillonite, illite and kaolinite. Appl Geochem. 2008;23:3840–51.
24. Klevtsov DP, Logvinenko VA, Zolotovskii BP, Krivoruchko OP, Buyanov RA. Kinetics of kaolinite dehydration and its dependence on mechanochemical activation. J Therm Anal. 1988;33:531–5.
25. Adhikaria M, Majumdara MK, Pati AK. Thermal Decomposition of Vermiculites: Kinetics of Dehydration and Dehydroxylation Processes. Trans Ind Ceram Soc. 1983;42(5)124–7.
26. Murray P, White J. Kinetics of clay dehydration. Clay Miner. 1955;2:255–64.
27. Vyazovkin S, Burnham AK, Criado JM, Pérez-Maqueda LA, Popescu C, Sbirrazzuoli N.

ICTAC Kinetic Committee recommendations for performing kinetic computations on thermal analysis data. Thermochim Acta 2011;520:1–19.

28. Liu H, Chen T, Xie Q, Zou X, Qing C, Frost RL. Kinetic study of goethite dehydration and the effect of aluminium substitution on the dehydrate. Thermochim Acta 2012;545:20–5.

29. Brown ME, Dollimore D, Galwey AK. Reactions in the Solid State. Comprehensive Chemical Kinetics, Vol. 22, Amsterdam; Elsevier; 1980.

30. Sestak J. Thermophysical Properties of Solids. Comprehensive Analytical Chemistry, Vol. 12D, Amsterdam; Elsevier; 1984.

31. Blaine RL, Hahn BK. Obtaining kinetic parameters by modulated thermogravimetry. J Therm Anal. 1998;54:695–704.

32. Brown ME, Maciejewski M, Vyazovkin S, Nomen R, Sempere J, Burnham A, Opfermann J, Strey R, Anderson HL, Kemmler A, Keuleers R, Janssens J, Desseyn HO, Li CR, Tang TB, Roduit B, Malek J, Mitsuhashi T. Computational aspects of kinetic analysis Part A: The ICTAC kinetics project-data, methods and results. Thermochim Acta 2000;355:125–43.

33. Flynn JH, Wall LA. A quick direct method for the determination of activation energy from thermogravimetric data. J Polym Sci B: Polym Lett. 1966;4(5):323–8.

34. Ozawa T. A new method of analyzing thermogravimetric data. Bull Chem Soc Jpn. 1965;38:1881–6.

35. Doyle CD. Estimating isothermal life from thermogravimetric data. J Appl Polym Sci. 1962;6(24):639–42.

36. Akahira T, Sunose T. Paper No. 246, 1969 Research Report, Trans. Joint Convention of Four Electrical Institutes. Chiba Inst Technol (Sci. Technol.) 1971;16:22–31.

37. Starink MJ. The determination of activation energy from linear heating rate experiments: a comparison of the accuracy of isoconversion methods, Thermochim Acta 2003;404:163–76.

38. Lesnikovich AI, Levchik SV. Isoparametric kinetic relations for chemical transformations in condensed substances (Analytical survey). II. Reactions involving the participation of solid substances. J Therm Anal. 1985;30:677–702.

39. Lesnikovich AI, Levchik SV. A method of finding invariant values of kinetic parameters, J. Therm. Anal. 1983;27:89–93.

40. Pérez-Maqueda LA, Criado JM, Sánchez-Jiménez PE, Perejón A. Kinetic studies in solid state reactions by sample-controlled methods and advanced analysis procedures. J Therm Anal Calorim. 2013;113:1447–53.

41. Pérez-Maqueda LA, Criado JM, Gotor FJ, Málek J. Advantages of Combined Kinetic Analysis of Experimental Data Obtained under Any Heating Profile. J Phys Chem A 2002;106:2862–8.
42. Vyazovkin S, Wight CA. Kinetics in solids. Annu Rev Phys Chem. 1997;48:125–49.
43. Simon P. Isoconversional methods. Fundamentals, meaning and application. J Therm Anal Calorim. 2004;74:123–32.
44. Vyazovkin S. Evaluation of the activation energy of thermally stimulated solid-state reactions under an arbitrary variation of the temperature. J Comput Chem. 1997;18:393–402.
45. Vyazovkin S. Modification of the integral isoconversional method to account for variation in the activation energy. J Comput Chem. 2001;22:178–183.
46. Vyazovkin S, Dollimore D. Linear and non linear procedures in isoconversional computations of the activation energy of thermally induced reactions in solids, J Chem Inf Comp Sci. 1996;36:42–5.
47. Budrugeac P, Segal E. Thermal analysis in the evaluation of thermal lifetime of solid polymeric materials. Thermochim Acta 1992;211:131–6.
48. Coats AW, Redfern JP. Kinetic parameters for thermogravimetric data. Nature 1964;201:68–9.
49. Garcia FJ, Rodríguez SG, Kalytta A, Reller A. Study of Natural Halloysite from the Dragon Mine, Utah (USA). Z Anorg Allg Chem. 2009;635(4‐5):790–5.
50. Badogiannis E, Kakali G, Tsivilis S. Metakaolin as supplementary cementitious material. Optimization of kaolin to metakaolin conversion. J Therm Anal Calorim. 2005;81:457–62.
51. NIST Chemistry WebBook Standard Reference Database, http://webbook.nist.gov/chemistry
52. da Silveira Petruci JF, Fortes PR, Kokoric V, Wilk A, Raimundo Jr. IM, Cardoso AA, Mizaikoff B. Monitoring of hydrogen sulfide via substrate-integrated hollow waveguide mid-infrared sensors in real-time. Analyst 2014;139:198–203.
53. Heide K, Foldvari M. High temperature mass spectrometric gas-release studies of kaolinite $Al_2[Si_2O_5(OH)_4]$ decomposition. Thermochim Acta 2006;446:106–12.
54. Prado JR, Vyazovkin S. Activation energies of water vaporization from the bulk and from laponite, montmorillonite, and chitosan powders. Thermochim Acta 2011;524:197–201.

Table 1 Comparison of experimental DTG peak temperatures T_p and mass loss percentages for all the steps evaluated from the TG curves performed at 10 °C min^{-1} under a stream of air for all the investigated materials

Process	T_p /°C			Mass Lo	
	HNTs	etched HNTs	KAO	HNTs	etched
Dehydration (step 1)	37.5	39.5	n.d.	2.3	4.
Dehydration (step 2)	245	n.d.	n.d.	3.3	n.d
Dehydroxylation	468	479	503	11.4	6.
Thermal Decomposition (loss of sulfide)	744	730	n.d.	1.7	3.

n.d. = not detected

Captions of the figures

Fig. 1 *a* STEM image of pristine HNTs, *b* STEM image of etched HNTs, *c* SEM image of pristine HNTs, *d* SEM image of etched HNTs.

Fig. 2 *a* TG and *b* DTG curves of the materials investigated under a stream of air at 10 °C min^{-1}.

Fig. 3 FTIR spectra of gases evolved during the TG experiments at *a* 39, 245 and 468°C, *b* and 750°C.

Fig. 4 Isoconversional dependency of activation energy of dehydration (loss of layered water molecules) occurring in pristine HNTs according to the different kinetic methods

Fig. 5 Isoconversional dependencies of activation energy of dehydroxylation (condensation of water due to dehydroxylation of hydroxyl groups of alumina inner sheets) according to the different kinetic methods for *a* HNTs , *b* etched HNTs, *c* KAO.

468

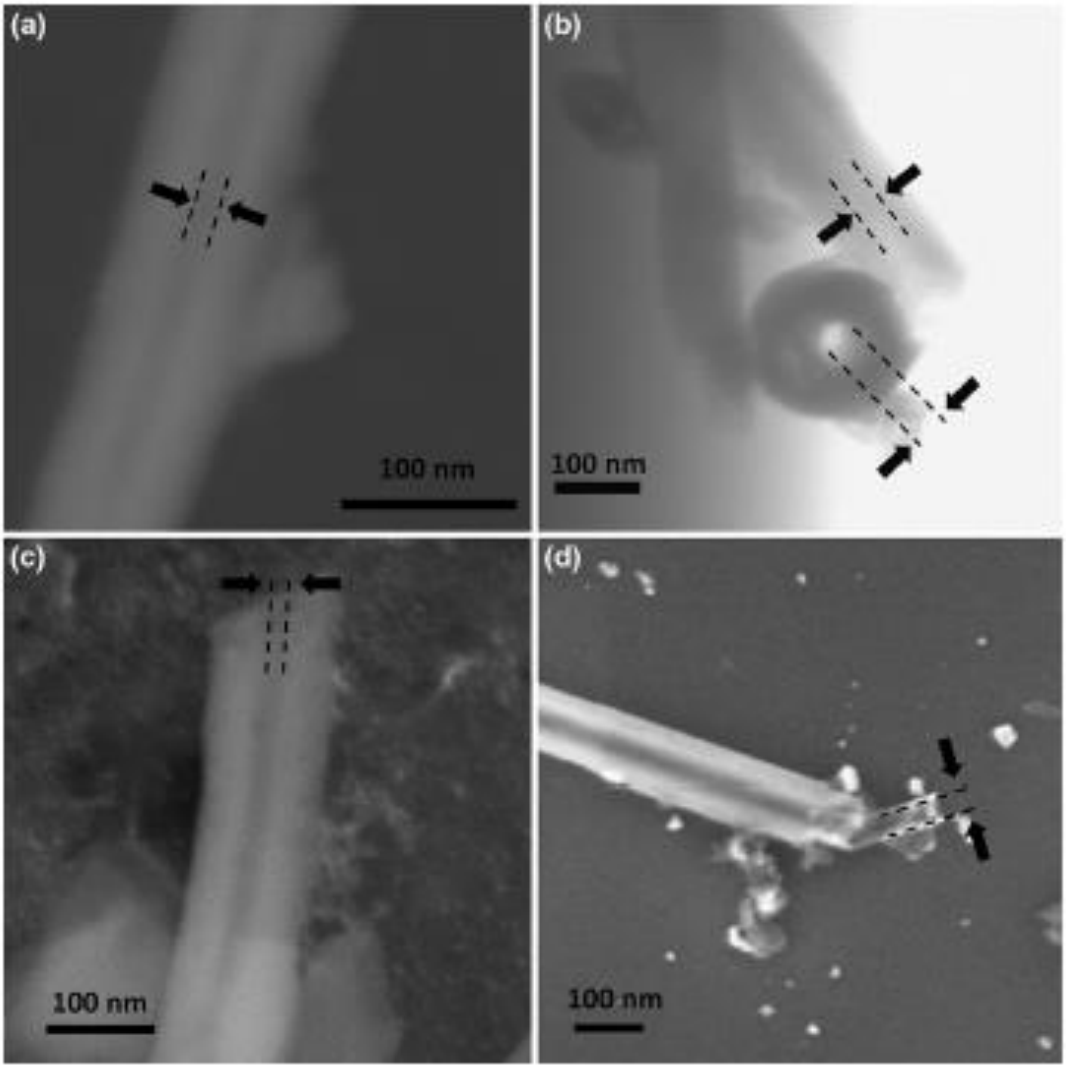

469

470

471

472

473

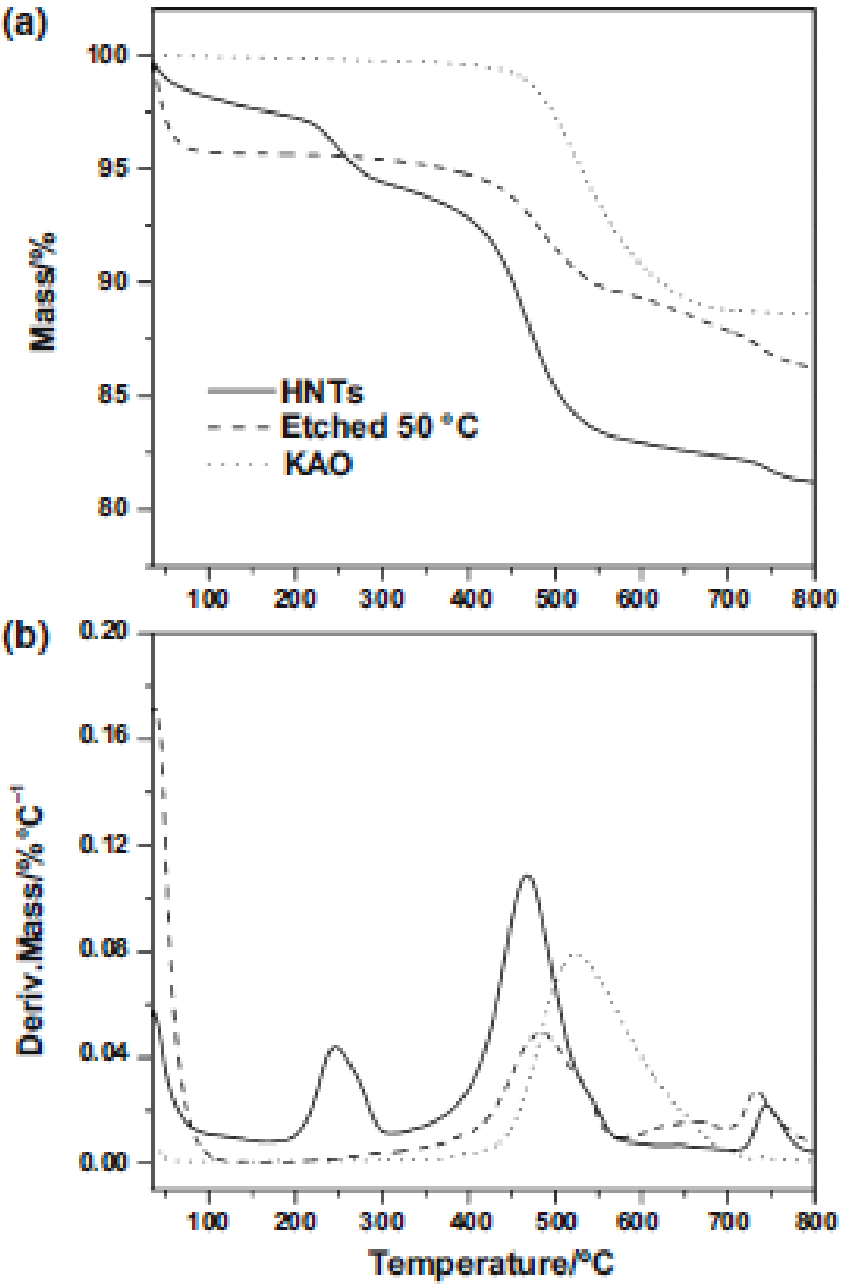
(a)
100
95
90
85
80
Mass/%
HNTs
Etched 50 °C
KAO
100
200
300
400
500
600
700
800
(b)
0.20
0.16
0.12
0.08
0.04
0.00
Deriv.Mass/% °C⁻¹
100
200
300
400
500
600
700
800
Temperature/°C

474

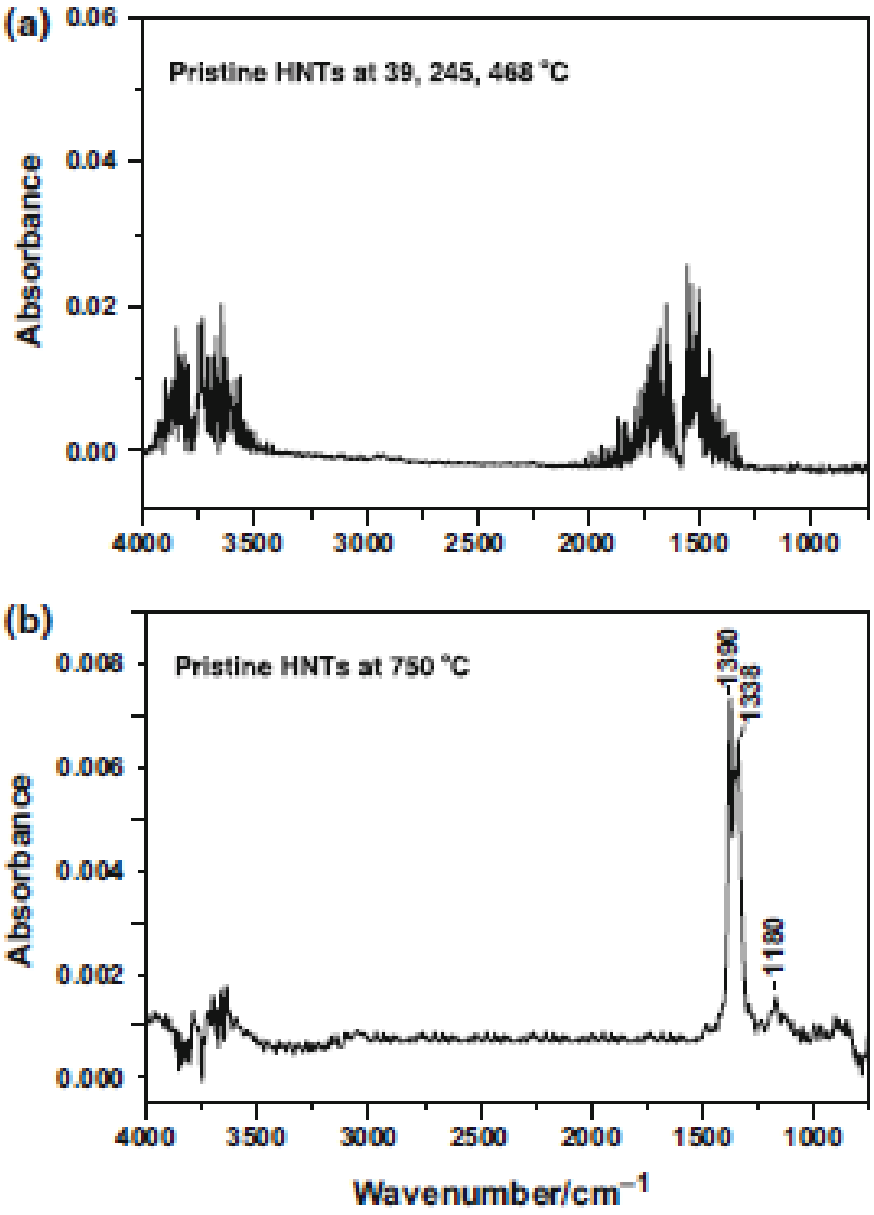
(a)
Pristine HNTs at 39, 245, 468 °C
Absorbance
0.06
0.04
0.02
0.00
4000
3500
3000
2500
2000
1500
1000
(b)
Pristine HNTs at 750 °C
1390
1338
1180
Absorbance
0.008
0.006
0.004
0.002
0.000
4000
3500
3000
2500
2000
1500
1000
Wavenumber/cm^{-1}

475

476

477

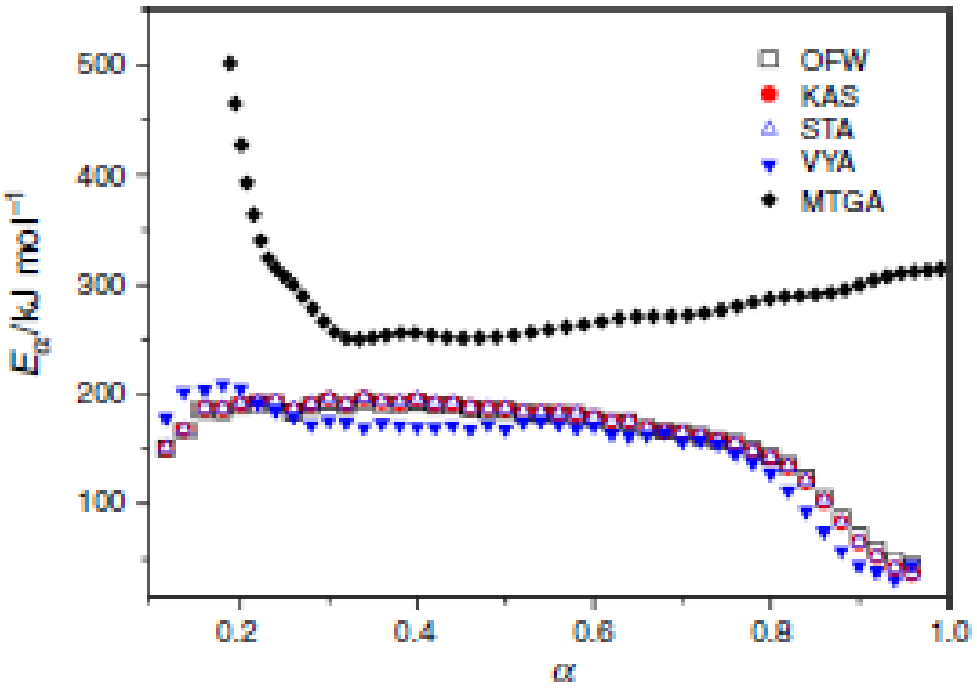
OFW
KAS
STA
VYA
MTGA
500
400
300
200
100
0.2
0.4
0.6
0.8
1.0
α
E_α/kJ mol^{-1}

478

479

480

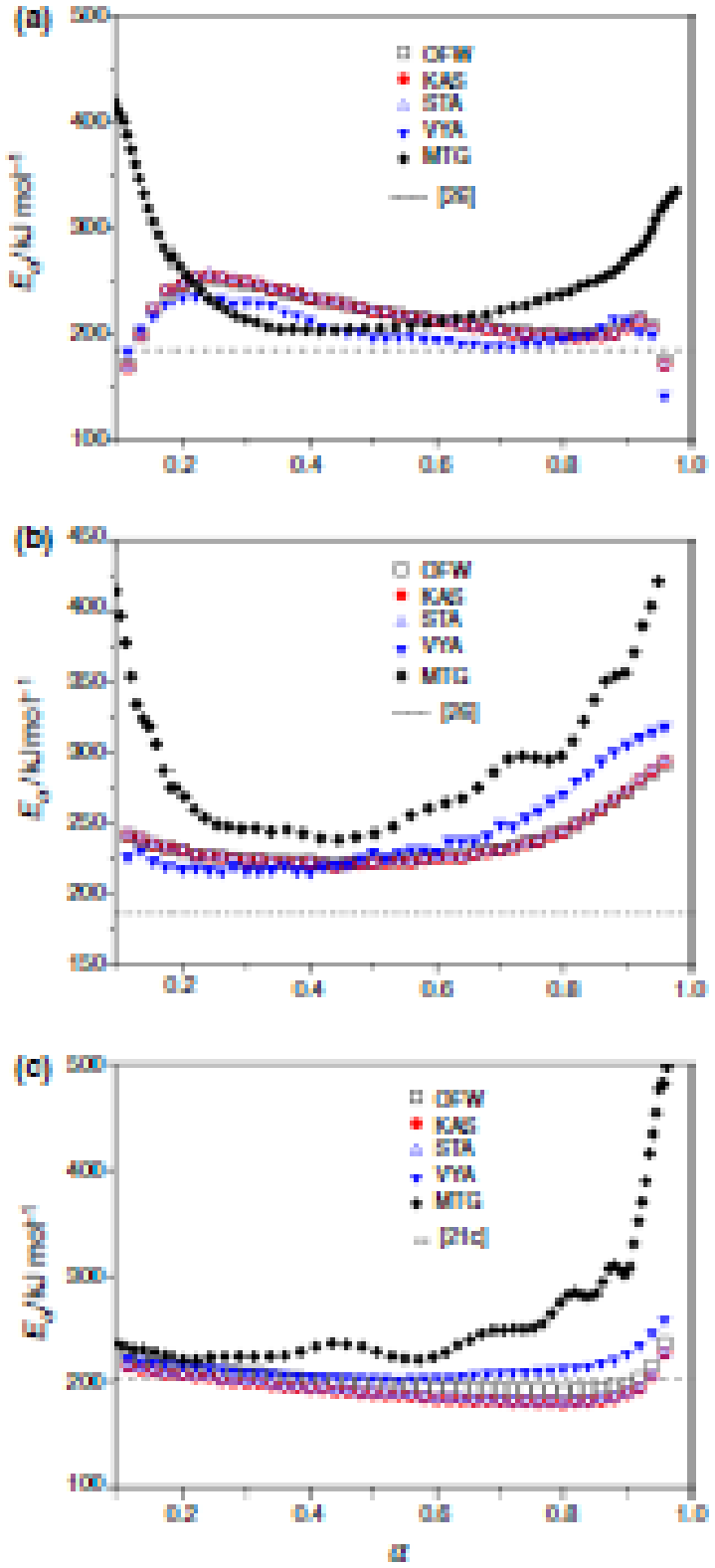
(a)
OFW
KAS
STA
VYA
MTG
[26]
E_α/kJ mol^{-1}
(b)
OFW
KAS
STA
VYA
MTG
[26]
E_α/kJ mol^{-1}
(c)
OFW
KAS
STA
VYA
MTG
[21c]
E_α/kJ mol^{-1}
α

481

482